Highly nonlinear dynamics of third-harmonic generation by focused beams

Richard S. Tasgal,[1] Marek Trippenbach,[2] M. Matuszewski,[2] and Y. B. Band[1]
[1]*Departments of Chemistry and Electro-Optics, Ben-Gurion University of the Negev, Beer-Sheva 84105, Israel*
[2]*Institute of Experimental Physics, Optics Division, Warsaw University, ul. Hoża 69, Warsaw 00-681, Poland*
(Received 6 August 2003; published 16 January 2004)

Beams that experience third-harmonic generation (THG) also experience Kerr effects. With Kerr effects, beams do not take simple Gaussian shapes, but exhibit nonlinear dynamics. These nonlinear dynamics have an effect on the THG accumulated by focusing and then diverging beams. We formulate a self-consistent and complete set of nonlinear Schrödinger equations for a pair of coupled beams—a fundamental and its third-harmonic. Numerical simulations show that the Kerr nonlinearities allow some third harmonic to propagate to the far-field even for zero or negative phase mismatch. This is because the nonlinear dynamics break the beams' reflection symmetry about the focal plane and therefore increases far-field THG by changing some of the interference from destructive to constructive. THG conversion efficiencies are computed as functions of several beam parameters.

DOI: 10.1103/PhysRevA.69.013809 PACS number(s): 42.65.Jx, 42.65.Sf, 42.65.Ky, 42.25.Ja

I. INTRODUCTION

We study the dynamics of two-color beams in a nonlinear isotropic medium. We take the initial conditions to be a one-color beam with Gaussian profile. With a cubic ($\chi^{(3)}$) nonlinearity, which is the lowest order possible in an isotropic medium, the possible nonlinearities are third-harmonic generation (THG), Kerr, and Raman. Any other nonlinearity requires either a different susceptibility (second-harmonics, high-harmonics), or more than two slowly-varying envelopes (sum and difference frequency generation). This is one of the simplest nonlinear optics problems, and is for that reason important; it has an application to THG microscopy [1].

The usual model of THG takes the fundamental beam to be Gaussian, and (inconsistently, or as an approximation) has THG as the sole nonlinearity [2,3]. This model has an exact analytic solution in which the third-harmonic (TH) beam takes a Gaussian profile. For a phase mismatch that is zero or negative, the energy in the TH peaks at the focus of the fundamental beam, and, after the focus, destructive interference causes *all* the TH to be reabsorbed by the fundamental. The latter is often said to be due to the Guoy shift [3], the phase shift of π that a Gaussian beam experiences in going from a far-field, through a focus, to a far-field. But, in fact, the details show it to depend on the beam's phase and shape everywhere along its path. However, the fast (electronic) nonlinear response of optical materials that yields THG also generates Kerr effects (self- and cross-phase modulations). Therefore, one should include Kerr and perhaps also Raman effects when modeling THG. These can have quite drastic effects on a beam [4]. Although it was recognized as early as 1973 that Kerr effects could influence THG [5], and although Kerr, THG, and dispersion have been examined in studies *without* transverse spatial dynamics [6,7], the results of transverse nonlinear dynamics on THG have not heretofore been studied in quantitative detail.

We have derived a set of coupled nonlinear Schrödinger (NLS) equations for two slowly-varying envelopes, with the relevant nonlinearities treated rigorously and consistently [8]. Because of the microscopy application, we are interested in very tightly focused beams and pulses, with large momentum and frequency spreads. The NLS equations are thus given to all orders in dispersion and diffraction; numerical simulations are carried out with a method that is accurate to all orders relevant for the grid [9–11]. We express the field as a fundamental, $A_\omega(\mathbf{x},t)$, centered about a carrier wave at frequency ω_0, and a TH, $A_{3\omega}(\mathbf{x},t)$, centered about a carrier wave at frequency $3\omega_0$:

$$-i\partial_z A_\omega(\mathbf{x},t)=\left[\sum_{p=1}^{\infty}\frac{i^p}{p!}\left(\frac{\partial^p}{\partial\omega^p}\beta(\omega)\right)_{\omega_0}\partial_t^p-\sum_{m=1}^{\infty}\frac{(2m-3)!!}{(-2)^m m!}\frac{\Delta_\perp^m}{\beta(\omega_0)^{2m-1}}\right.$$
$$\left.-\sum_{p,m=1}^{\infty}\frac{i^p(2m-3)!!}{(-2)^m m!p!}\left(\frac{\partial^p}{\partial\omega^p}\frac{1}{\beta(\omega)^{2m-1}}\right)_{\omega_0}\Delta_\perp^m\partial_t^p\right]A_\omega$$
$$+\sum_{p,m=0}^{\infty}2\pi\frac{i^p(2m-1)!!}{(-2)^m m!p!}\left(\frac{\partial^p}{\partial\omega^p}\frac{(\omega/c)^2}{\beta(\omega)^{2m+1}}\right)_{\omega_0}\Delta_\perp^m\partial_t^p P_\omega(\mathbf{x},t), \tag{1a}$$

$$-i\partial_z A_{3\omega}(\mathbf{x},t)=\left[\sum_{p=1}^{\infty}\frac{i^p}{p!}\left(\frac{\partial^p}{\partial\omega^p}\beta(\omega)\right)_{3\omega_0}\partial_t^p-\sum_{m=1}^{\infty}\frac{(2m-3)!!}{(-2)^m m!}\frac{\Delta_\perp^m}{\beta(3\omega_0)^{2m-1}}\right.$$
$$\left.-\sum_{p,m=1}^{\infty}\frac{i^p(2m-3)!!}{(-2)^m m!p!}\left(\frac{\partial^p}{\partial\omega^p}\frac{1}{\beta(\omega)^{2m-1}}\right)_{3\omega_0}\Delta_\perp^m\partial_t^p\right]A_{3\omega}$$
$$+\sum_{p,m=0}^{\infty}2\pi\frac{i^p(2m-1)!!}{(-2)^m m!p!}\left(\frac{\partial^p}{\partial\omega^p}\frac{(\omega/c)^2}{\beta(\omega)^{2m+1}}\right)_{3\omega_0}\Delta_\perp^m\partial_t^p P_{3\omega}(\mathbf{x},t). \tag{1b}$$

In the NLS equations (1), $\Delta_\perp\equiv\partial_x^2+\partial_y^2$ is the transverse Laplacian, $n(\omega)$ is the index of refraction at frequency ω, and $\beta(\omega)\equiv n(\omega)\omega/c$ is the wavenumber. The first summation terms on the right-hand sides of Eqs. (1) are dispersion, the second summation is diffraction, the third summation is cross-dispersion/diffraction. The nonlinear polarization includes THG, Kerr, and Raman effects [3,7,12]. Self-steepening terms [13,14], of the form $\partial(|A|^2A)/\partial t$ and self-frequency shifting terms of the form $(\partial|A|^2/\partial t)A$ are contained in the first-order time derivatives of the nonlinear polarizations $P_\omega(\mathbf{x},t)$ and $P_{3\omega}(\mathbf{x},t)$ in Eqs. (1). The NLS equations (1) show that self-steepening terms and self-frequency shifting terms are just the first terms of a family of higher order nonlinear terms.

The nonlinear polarization is taken to be of the form

$$P_\omega(\mathbf{x},t)=3\chi^{\mathrm{elec}}(-\omega_0;-\omega_0,-\omega_0,3\omega_0)\exp\{-i[3\beta(\omega_0)-\beta(3\omega_0)]z\}A_\omega(\mathbf{x},t)^{*2}A_{3\omega}(\mathbf{x},t)$$
$$+3\chi^{\mathrm{elec}}(-\omega_0;\omega_0,-\omega_0,\omega_0)|A_\omega(\mathbf{x},t)|^2A_\omega(\mathbf{x},t)+6\chi^{\mathrm{elec}}(-\omega_0;3\omega_0,-3\omega_0,\omega_0)|A_{3\omega}(\mathbf{x},t)|^2A_\omega(\mathbf{x},t)$$
$$+A_\omega(\mathbf{x},t)\int_0^\infty[3\chi^{\mathrm{nucl}}(-\omega_0;\omega_0,-\omega_0,\omega_0;s)|A_\omega(\mathbf{x},t-s)|^2+3\chi^{\mathrm{nucl}}(-\omega_0;\omega_0,-3\omega_0,3\omega_0;s)|A_{3\omega}(\mathbf{x},t-s)|^2]ds$$
$$+A_{3\omega}(\mathbf{x},t)\int_0^\infty\exp(-2i\omega_0 s)3\chi^{\mathrm{nucl}}(-\omega_0;3\omega_0,-\omega_0,-3\omega_0;s)A_\omega(\mathbf{x},t-s)A_{3\omega}(\mathbf{x},t-s)^*ds, \tag{2a}$$

$$P_{3\omega}(\mathbf{x},t)=\chi^{\mathrm{elec}}(-3\omega_0;\omega_0,\omega_0,\omega_0)\exp\{i[3\beta(\omega_0)-\beta(3\omega_0)]z\}A_\omega(\mathbf{x},t)^3+6\chi^{\mathrm{elec}}(-3\omega_0;\omega_0,-\omega_0,3\omega_0)|A_\omega(\mathbf{x},t)|^2A_{3\omega}(\mathbf{x},t)$$
$$+3\chi^{\mathrm{elec}}(-3\omega_0;3\omega_0,-3\omega_0,3\omega_0)|A_{3\omega}(\mathbf{x},t)|^2A_{3\omega}(\mathbf{x},t)+A_{3\omega}(\mathbf{x},t)\int_0^\infty[3\chi^{\mathrm{nucl}}(-3\omega_0;\omega_0,-\omega_0,3\omega_0;s)$$
$$\times|A_\omega(\mathbf{x},t-s)|^2+3\chi^{\mathrm{nucl}}(-3\omega_0;3\omega_0,-3\omega_0,3\omega_0;s)|A_{3\omega}(\mathbf{x},t-s)|^2]ds+A_\omega(\mathbf{x},t)\int_0^\infty\exp(2i\omega_0 s)$$
$$\times3\chi^{\mathrm{nucl}}(-3\omega_0;\omega_0,-\omega_0,3\omega_0;s)A_\omega(\mathbf{x},t-s)^*A_{3\omega}(\mathbf{x},t-s)ds. \tag{2b}$$

This breaks up the nonlinear response into an electronic (fast) part and a nuclear (slow) part. It also assumes that the electronic part of the response may be considered frequency-independent on the scale of the pulse bandwidths; it does not make this assumption for the nuclear part of the response. For the calculations, we take a more specific nonlinear polarization, essentially the standard model of the third-order susceptibility of fused silica [12,15–17] plus a generalization:

$$P_\omega(\mathbf{x},t)=\exp\{-i[3\beta(\omega_0)-\beta(3\omega_0)]z\}\chi^{\mathrm{THG}}A_\omega(\mathbf{x},t)^{*2}A_{3\omega}(\mathbf{x},t)+\chi^{\mathrm{elec}}(|A_\omega(\mathbf{x},t)|^2+2|A_{3\omega}(\mathbf{x},t)|^2)A_\omega(\mathbf{x},t)$$
$$+A_\omega(\mathbf{x},t)\int_0^\infty\chi^{\mathrm{nucl}}(s)(|A_\omega(\mathbf{x},t-s)|^2+|A_{3\omega}(\mathbf{x},t-s)|^2)ds+A_{3\omega}(\mathbf{x},t)\int_0^\infty\exp(-2i\omega_0 s)\chi^{\mathrm{nucl}}(s)A_\omega(\mathbf{x},t-s)$$
$$\times A_{3\omega}(\mathbf{x},t-s)^*ds, \tag{3a}$$

$$P_{3\omega}(\mathbf{x},t)=\exp\{i[3\beta(\omega_0)-\beta(3\omega_0)]z\}\frac{1}{3}\chi^{\mathrm{THG}}A_\omega(\mathbf{x},t)^3+\chi^{\mathrm{elec}}(2|A_\omega(\mathbf{x},t)|^2+|A_{3\omega}(\mathbf{x},t)|^2)A_{3\omega}(\mathbf{x},t)$$
$$+A_{3\omega}(\mathbf{x},t)\int_0^\infty\chi^{\mathrm{nucl}}(s)(|A_\omega(\mathbf{x},t-s)|^2+|A_{3\omega}(\mathbf{x},t-s)|^2)ds+A_\omega(\mathbf{x},t)\int_0^\infty\exp(2i\omega_0 s)\chi^{\mathrm{nucl}}(s)$$
$$\times A_\omega(\mathbf{x},t-s)^*A_{3\omega}(\mathbf{x},t-s)ds. \tag{3b}$$

Here the THG coefficient is decoupled from the other electronic susceptibilities; this is outside the usual model for pure fused silica in which the electronic contribution is considered instantaneous and the nuclear contribution takes the form arising from a single damped harmonic oscillator,

$$\chi(t;t_1,t_2,t_3)=\chi^{\mathrm{elec}}\delta(t-t_1)\,\delta(t_1-t_2)\,\delta(t_2-t_3)+\chi^{\mathrm{nucl}}(t_1-t_2)\,\delta(t-t_1)\,\delta(t_2-t_3),$$

with $\chi^{\mathrm{elec}}=n_2(1-f_{\mathrm{Raman}})$, $\chi^{\mathrm{nucl}}(t)=n_2 f_{\mathrm{Raman}}(\tau_1^2+\tau_2^2)\tau_1^{-1}\tau_2^{-2}\exp(-t/\tau_2)\sin(t/\tau_1)$, $n_2=n(\omega)cn_2^I/(2\pi)$, $n_2^I=2.8\times10^{-20}$ m^2/W, $f_{\mathrm{Raman}}=0.18$, $\tau_1=12.2$ fs, and $\tau_2=32.0$ fs. If the electronic THG susceptibility differs from the other electronic susceptibilities, the electronic contribution to the susceptibility is not instantaneous compared to all scales. Direct experimental measurements of the THG susceptibilities are available [18–20]. The more recent measurement of the THG coefficient χ^{THG} [19] is smaller than the electronic contribution to self-phase modulation [18] χ^{elec} by a factor of almost 4; older measurements [20] give a THG coefficient smaller than the electronic part of the self-phase modulation by a factor of about 1.5. In the absence of direct experimental measurements of all the nonlinear polarization coefficients for doped silica, we use the simplest case $\chi^{\mathrm{THG}}=\chi^{\mathrm{elec}}$ in numerical simulations, but discuss how the results scale for different values of the THG coefficient. Vector effects are neglected. Interband Raman scattering is negligible *at the carrier frequencies* because of the fast relative phase oscillation; but in the pulse simulations, inter-band Raman scattering is possible between the lower frequencies within the higher frequency band, and the higher frequencies within the lower frequency band.

II. NUMERICAL SIMULATIONS

A numerical NLS propagation scheme may be said to be accurate to all orders of dispersion and diffraction if it is accurate to as many orders as there are grid points. Accuracy up to all available orders requires the index of refraction over the entire numerically represented frequency range. In the split-step fast Fourier transform scheme, linear propagation is carried out in momentum space; the algorithm may be made accurate to all orders by putting the frequency dependent index of refraction directly into the formulas for the propagators [8], i.e.,

$$-i\partial_z A_\omega(\mathbf{x},t)=\mathcal{F}^{-1}\{[\sqrt{\beta(\omega_0+\omega)^2-k_\perp^2}-\beta(\omega_0)]\mathcal{F}\{A_\omega(\mathbf{x},t)\}\}+\mathcal{F}^{-1}\left\{\frac{2\pi(\omega_0+\omega)^2/c^2}{\sqrt{\beta(\omega_0+\omega)^2-k_\perp^2}}\mathcal{F}\{P_\omega(\mathbf{x},t)\}\right\},\tag{4a}$$

$$-i\partial_z A_{3\omega}(\mathbf{x},t)=\mathcal{F}^{-1}\{[\sqrt{\beta(3\omega_0+\omega)^2-k_\perp^2}-\beta(3\omega_0)]\mathcal{F}\{A_{3\omega}(\mathbf{x},t)\}\}+\mathcal{F}^{-1}\left\{\frac{2\pi(3\omega_0+\omega)^2/c^2}{\sqrt{\beta(3\omega_0+\omega)^2-k_\perp^2}}\mathcal{F}\{P_{3\omega}(\mathbf{x},t)\}\right\}.\tag{4b}$$

Here $\mathcal{F}$ and $\mathcal{F}^{-1}$ are Fourier and inverse Fourier transforms in x,y,t, $k_\perp=\sqrt{k_x^2+k_y^2}$ is the transverse momentum, and ω is frequency. The linear dispersion effects are contained in $\beta(\omega)=n(\omega)\omega/c$; diffraction is contained in $k_\perp$. The offsets by ω_0 and $3\omega_0$ are due to the fact that the fields are slowly varying envelopes about carrier waves at those frequencies; when these appear, ω is the frequency relative to the offset. There is no need to compute the coefficients for dispersion, diffraction, self-steepening, *etc.*, explicitly because they are contained implicitly in the linear dispersion $\beta(\omega)$. Since we simulate focusing and collapse, during which diffractive, dispersive, and nonlinear length scales can easily change by factors of a hundred or more [12,14], we allow the propagation step to vary such that it remains an order of magnitude less that the smallest relevent scale.

The effects that we are interested in are larger and clearer when the fundamental and TH are not too far from being phase matched, $\Delta k\equiv3\beta(\omega_0)-\beta(3\omega_0)\approx0$, or $n(\omega_0)\approx n(3\omega_0)$. Optical materials may be doped to obtain desired properties [12,21]. We consider silica doped with neodynium to obtain an approximate phase matching between the fundamental $\lambda=1.5$ μm and TH $\lambda=0.5$ μm. To model the frequency dependent index of refraction, we use the Sellmeier relation for fused silica [22], but add one additional resonance at $\lambda_{\mathrm{Nd}}=0.59$ μm, which is neodynium's largest resonance in the vicinity of our TH. For this, phase matching is achieved at the Sellmeier coefficient $B_{\mathrm{Nd}}\approx0.0138$, which corresponds to a few percent doping of the material. Phase mismatch is varied by changing the dopant concentration (in this model, the Sellmeier coefficient B_{Nd}). We take the conventional nonlinear coefficients for pure silica [12], as given above.

We simulated the propagation of both pulses and continuous beams, over a range of light intensities, phase-mismatch values, and focusing strengths. The effects of the nonlinearity are clearly visible in Fig. 1, which shows the evolution of beams with varying intensity. For all simulations, we took initial conditions with zero power in the TH, and the fundamental in the form of a Gaussian with some radial phase factor $A_1(x,t;z=0)=A_1\exp[-(ic_1+2\ln2/W_1^2)(x^2+y^2)]$. The radial phase factor c_1 can be related to the wave front radius of curvature R_1 via the magnitude of the wavevector $\beta(\omega)=n(\omega)\omega/c$ according to the formula $R_1=0.5\beta(\omega)/c_1$. Because the fundamental focuses very intensely, while only a relatively small part of it is converted to TH, we illustrate the *peak intensity* of the fundamental beam and the *power* of the TH beam. In Fig. 1, the input beam has an initial full width at half maximum of 50 μm, a radial phase factor $c_1=5.0\times10^9/\mathrm{m}^2$ that brings the beam to a focus in 0.6 mm, and the material is phase matched (the reciprocal of the phase mismatch is more than an order of magnitude greater than the simulation distance). The fact that the *normalized* TH power varies with fundamental input intensity shows that the beams experience nonlinear dynamics, changing shape as the intensity changes. In Fig. 1, the initial wave front radii of curvature are small and their effect on the position of the focus overshadow the intensity dependence. One can see that the beams approach the linear limit at low in-

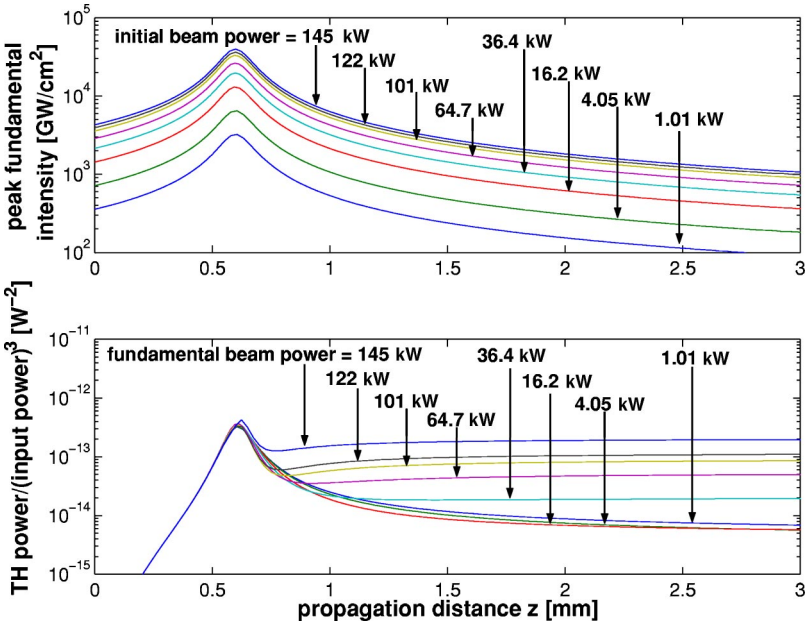

FIG. 1. Peak intensity of the fundamental ($\lambda_1 = 1.5\ \mu$m) beam, and power of the third harmonic ($\lambda_3 = 0.5\ \mu$m) normalized by the cube of the input power. The initial conditions have a range of intensities (1.01, 4.05, 16.2, 36.4, 64.7, 101, 122, and 145 kW, corresponding to circled points in the appropriate curve in Fig. 2), but an identical beam width, a full width at half maximum of 50 μm, radial phase factor, $c_1 = 5.0 \times 10^9/\mathrm{m}^2$ (i.e., transverse phase $\exp[-ic_1(x^2+y^2)]$), and all are phase matched.

tensities, as these curves start to almost overlap. Figure 2 shows the normalized *far-field* TH power as a function of input power, for the data in Fig. 1 and for another set of runs with weaker focusing.

For a qualitative explanation of these figures, we first contrast our results with the model in which THG is the only nonlinearity [2,3]. Here, in the case with phase matching, the TH power $P_{\mathrm{TH}}(z) = (3/2)(2\pi/nc)^2(\omega/c)^4(\pi W_1^2)^3\chi^{(3)2}I_\omega^3/[1+(z-z_{\mathrm{focus}})^2/z_1^2]$ reaches a maximum at the focus of the fundamental and then drops off as the inverse square of z/z_1, where $z_1 = \pi W_1^2/\lambda_0$ is the Rayleigh range of the fundamental *and* the TH beam, and W_1 is the width of the fundamental at its focus. Our simulations show that at high intensities, the Kerr effect causes the beams to lose reflection symmetry about the focal plane. With this asymmetry, THG from the incoming and outgoing beams does not fully interfere destructively, and allows some TH to propagate to the far-field. The lower-intensity curves in Fig. 1 do not quite drop off as the inverse square of distance because the numerical simulations did not start out from minus infinity, but began with merely a large (finite) beam width. The reflection asymmetry in Fig. 1 is due partly to the nonlinearities and partly to starting with a finite initial beam width. As long as the amount of energy in the TH is relatively small, the nonlinear dynamic effects will remain in the fundamental beam, and the TH peak intensities and beam powers may scale up or down by a uniform factor, but will be otherwise unaffected.

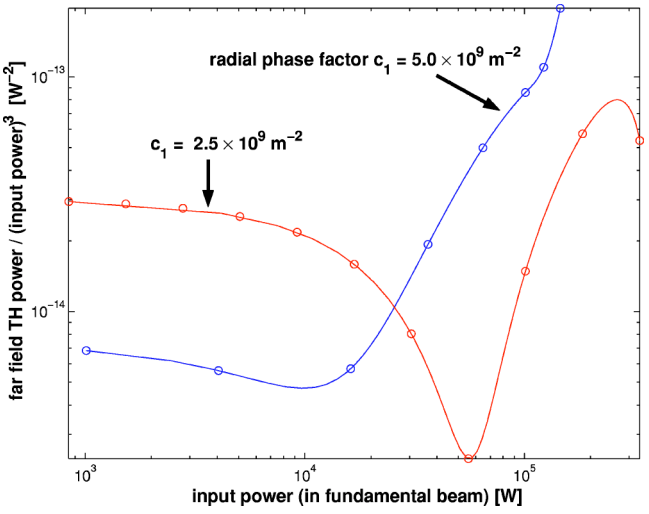

FIG. 2. Far-field third-harmonic beam power, normalized by the cube of the input power, vs input power. The medium has TH phase matching. Two curves are shown, one the far-field results from Fig. 1, and another with a smaller radial phase factor, that brings the beam to a focus in about 1.2 mm.

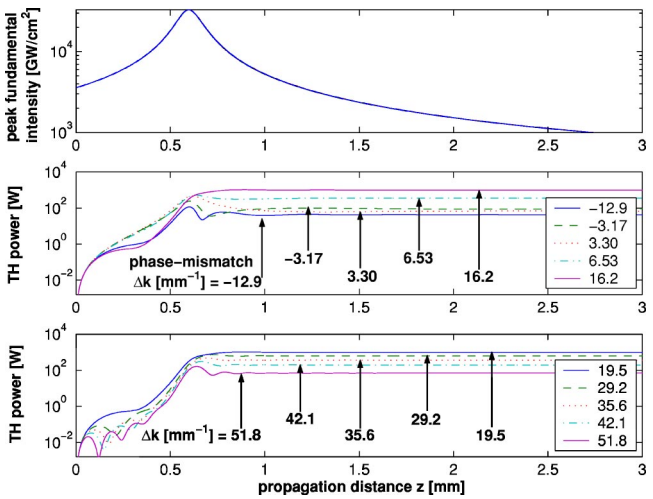

FIG. 3. Peak intensity of the fundamental beam, and power of the third harmonic. The curves represent beams with identical power, width, and radial phase factor, while the phase mismatch goes from -12.9 to 51.8 mm^{-1} (corresponding to circled points in the appropriate curve in Fig. 4). The middle plot shows the TH increasing with phase mismatch, and the bottom plot shows TH decreasing with phase mismatch.

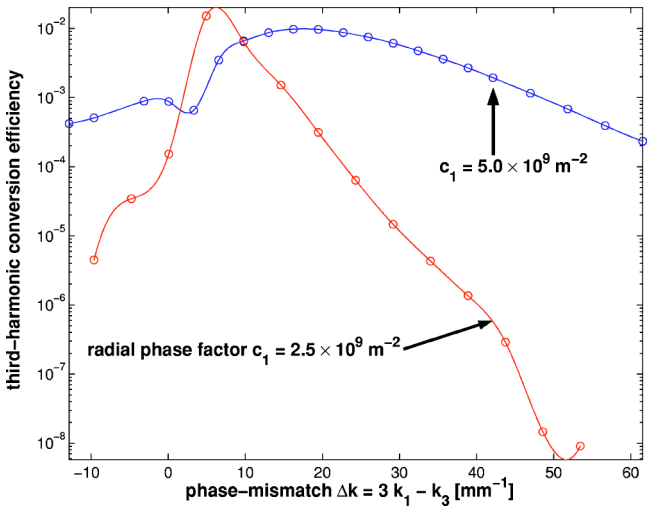

FIG. 4. Far-field conversion efficiency vs phase mismatch. Two curves are shown, one the far-field results from Fig. 3, and another with smaller radial phase factor, that brings the beam to a focus in about 1.2 mm. Initial intensities are held constant.

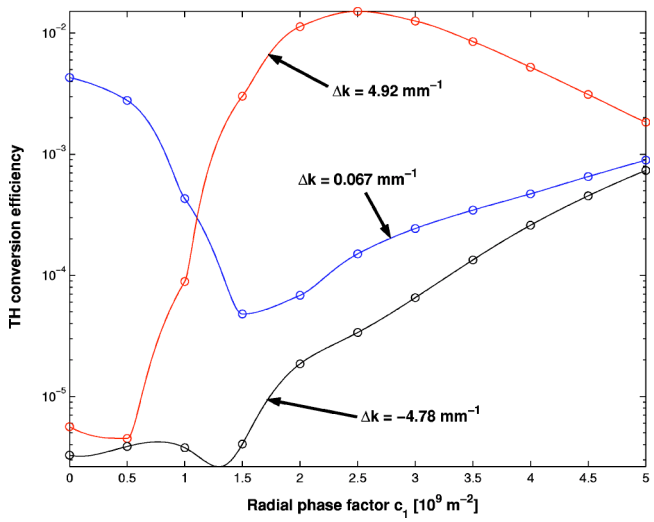

FIG. 6. Far-field conversion efficiency vs radial phase factor. Two curves are shown, one the far-field results from Fig. 5 (phase-matching), and another in a medium with positive phase-mismatching.

Clearly, there is significant variation with the fundamental input power. Moreover, this variation is quite different for different focusing conditions.

In another series of simulations, phase-mismatch is varied. Figure 3 shows the peak intensity of the fundamental and TH beam powers with an initial full width at half maximum of 50 μm, a radial phase factor $c_1 = 5.0 \times 10^9/\mathrm{m}^2$, and phase mismatch from -12.9 to 51.8 mm^{-1}. Because the TH power first increases and then decreases with phase mismatch, we show the former range on one plot and the latter on another. Clearly, there is a residual far-field TH and its power depends on phase mismatch. Figure 4 shows the far-field TH conversion efficiency as a function of phase mismatch, for the runs in Fig. 3 and another set of runs with weaker focusing, $c_1 = 2.5 \times 10^9/\mathrm{m}^2$. As in the linear model [2], THG by a focusing beam is maximized around a certain phase mismatch; but the nonlinear dynamics complicate the results considerably.

In a further series of simulations, the intensity and phase mismatch were held constant, and the radial phase factor varied. This mixes up a few physical effects, since initial conditions with small radial phase factors cannot be considered as starting from the far-field. Figure 5 has an extremely small phase mismatch ($\Delta k = 0.067$ mm^{-1}), and radial phase

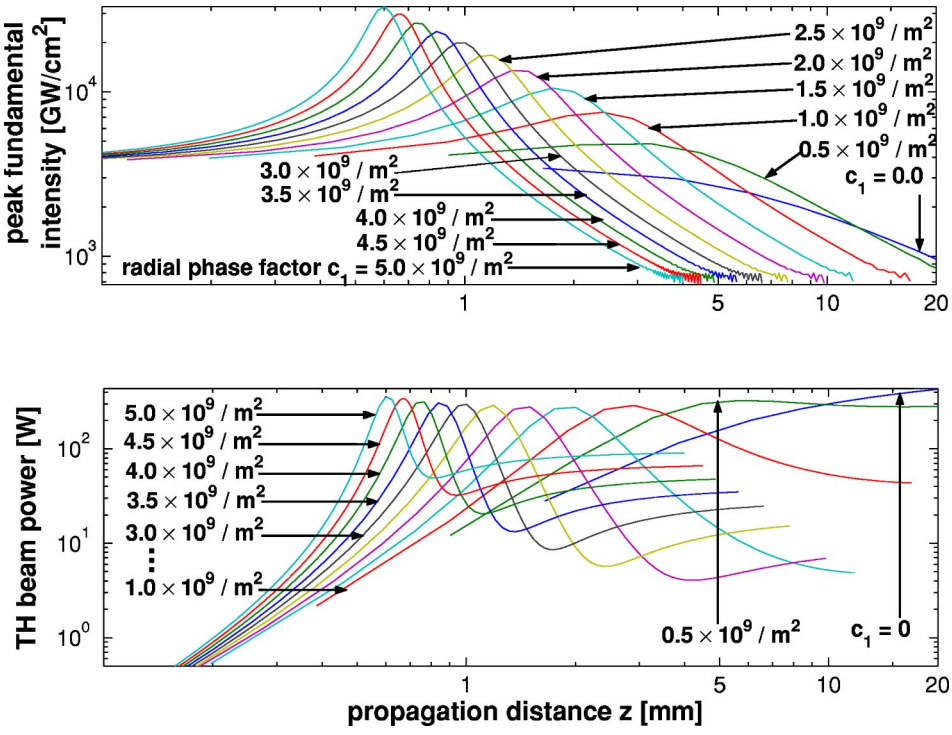

FIG. 5. Peak intensity of the fundamental beam, and power of the third-harmonic vs propagation distance for different fundamental radial curvatures. The curves show beams with phase matching and initially identical power and width; the initial radial phase factors go from zero (starting at a focus) up to $5.0 \times 10^9/\mathrm{m}^2$, by increments of $0.5 \times 10^9/\mathrm{m}^2$ (the curves here correspond to circled points in the appropriate curve in Fig. 6).

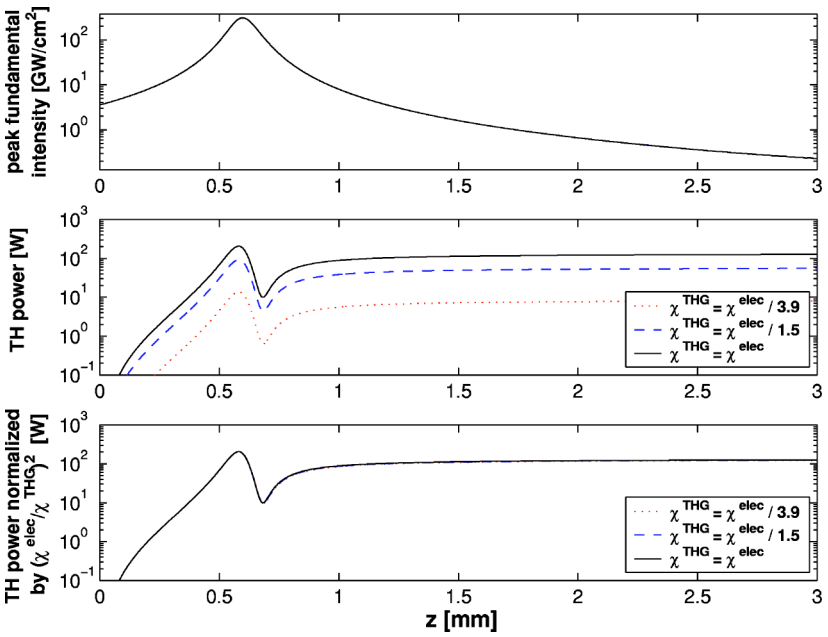

FIG. 7. Peak fundamental intensity and third-harmonic power vs position z, for various values of χ^{THG}. The third-harmonic power scales with $|\chi^{\mathrm{THG}}|^2$ when the third-harmonic intensity is small.

factors which vary from zero (i.e., starting at a focus) up to $c_1 = 5.0 \times 10^9/\mathrm{m}^2$. The horizontal axis is on a log scale to help visually distinguish the superimposed simulations. The peak fundamental intensity varies, but, over the range studied, the peak TH power is rather insensitive to the wave front radius of curvature of the fundamental, but the far-field TH power does vary considerably. Figure 6 shows the far-field TH power as a function of the radial phase factor, for the runs in Fig. 5, and also for a series of runs with significant positive and negative phase mismatch. In increasing (decreasing) the tightness of the focusing, the nonlinear and diffraction lengths both decrease (increase); the complexity of the results for far-field THG reflect the complexity of the nonlinear dynamics of the beam.

Figure 7 shows the dependence of the third-harmonic power on the when the THG susceptibility χ^{THG} is varied. The curve labeled $\chi^{\mathrm{THG}} = \chi^{\mathrm{elec}}$ corresponds to the same conditions used in Fig. 3 but with $\Delta k = 0.067\ \mathrm{mm}^{-1}$ (i.e., almost phase matched). The third-harmonic power scales with $|\chi^{\mathrm{THG}}|^2$ when the third-harmonic intensity is small since then the nonlinear dynamics of the fundamental is unaffected by TH and the generation of TH field is proportional to χ^{THG}. The values of χ^{THG} used in the calculations shown in Fig. 7 are factors of 1.0, 1/3.9, and 1/1.5 times the value used in the previous figures, where the latter two factors correspond to the measured values of χ^{THG} reported in Refs. [18–20].

Numerical simulations showed the dynamics of pulses to differ from those of continuous waves in essentially two ways. First, the group velocities of the fundamental and TH will, except for special cases, not be the same. A TH pulse will thus generally walk off from a fundamental pulse. This tends to reduce destructive interference; it also limits the effective distance over which the pulses interact. Compared to beams, TH pulses tend to carry off a larger part of the fundamental pulse energy. Secondly, the dynamics of pulses (3+1 dimensional) are qualitatively different to those of continuous beams (2+1 dimensional). For strongly focused but not very short pulses, these differences tend to be minor. A thorough analysis of focused pulses in this system is quite involved, and will be pursued elsewhere. Thus, the detailed results for continuous-wave beams apply to pulses for which group-velocity differences are relatively small or for pulses that are relatively long.

III. CONCLUSIONS

In a nonlinear medium, intense beams or pulses of finite diameter which converge to a focus and then diverge may exhibit nonlinear dynamics that significantly affect propagation dynamics. These nonlinear effects break the beam's reflection symmetry about the focal plane. The greater the intensity, the bigger the difference between incoming and outgoing beams. THG with such an input beam or pulse produces TH in the far-field when the phase-mismatch between the fundamental and its third-harmonic is zero or negative (and small). We have quantitatively demonstrated this for several cases. When phase-mismatch is positive, where some far-field TH power is possible in the essentially linear case, the nonlinear beam dynamics complicate the accumulation of TH power. The nonzero far-field THG for zero or negative phase mismatch—a qualitatively new effect for homogeneous media—is affected by, and thus contains information about, the medium in the region of the beam focus. For an inhomogeneous medium, and for THG microscopy, these effects should be understood, either to be utilized or better avoided.

ACKNOWLEDGMENTS

R. T. gratefully acknowledges financial support form the a Kreitman Foundation.This work was supported in part by a grant from the Israel Science Foundation for a Center of Excellence (Grant No. 8006/03) and by KBN Research Grant No. 2003-2006 (2P03B04325).

[1] Y. Barad, H. Eisenberg, M. Horowitz, and Y. Silberberg, Appl. Phys. Lett. **70**, 922 (1997); J.M. Schins, T. Schrama, J. Squier, G.J. Brakenhoff, and M. Muller, J. Opt. Soc. Am. B **19**, 1627 (2002).
[2] J.F. Ward and G.H.C. New, Phys. Rev. **185**, 57 (1969).
[3] R.W. Boyd, *Nonlinear Optics* (Academic, New York, 1992).
[4] L. Bergé, Phys. Rep. **303**, 259 (1998).
[5] R.B. Miles and S.E. Harris, IEEE J. Quantum Electron. **QE-9**, 470 (1973).
[6] Y.B. Band, Phys. Rev. A **42**, 5530 (1990).
[7] R.A. Sammut, A.V. Buryak, and Y.S. Kivshar, J. Opt. Soc. Am. B **15**, 1488 (1998).
[8] R.S. Tasgal and Y.B. Band (unpublished).
[9] M. Matuszewski, W. Wasilewski, M. Trippenbach, and Y.B. Band, Opt. Commun. **221**, 337 (2003); M. Trippenbach, W. Wasilewski, P. Kruk, G.W. Bryant, G. Fibich, and Y.B. Band, *ibid.* **210**, 385 (2002).
[10] J.E. Rothenberg, Opt. Lett. **17**, 1340 (1992).
[11] J.A. Fleck, J.R. Morris, and M.D. Feit, Appl. Phys. **10**, 129 (1976).
[12] G.P. Agrawal, *Nonlinear Fiber Optics* (Academic, San Diego, 1995).
[13] D. Anderson and M. Lisak, Phys. Rev. A **27**, 1393 (1983); P.V. Mamyshev and S.V. Chernikov, Opt. Lett. **15**, 1076 (1990); G. Fibich, Phys. Rev. Lett. **76**, 4356 (1996).
[14] M. Trippenbach and Y.B. Band, Phys. Rev. A **56**, 4242 (1997).
[15] R.W. Hellwarth, Prog. Quantum Electron. **5**, 1 (1977).
[16] R.H. Stolen, J.P. Gordon, W.J. Tomlinson, and H.A. Haus, J. Opt. Soc. Am. B **6**, 1159 (1989).
[17] K.J. Blow and D. Wood, IEEE J. Quantum Electron. **25**, 2665 (1989).
[18] D. Milam, Appl. Opt. **37**, 546 (1998).
[19] U. Gubler and C. Bosshard, Phys. Rev. B **61**, 10702 (2000).
[20] A. Mito, K. Hagimoto, and C. Takahashi, Nonlinear Opt. **13**, 3 (1995); C. Bosshard, U. Gubler, P. Kaatz, W. Mazerant, and U. Meier, Phys. Rev. B **61**, 10688 (2000).
[21] D.L. Nicacio, E.A. Gouveia, N.M. Borges, and A.S. Gouveia-Neto, Appl. Phys. Lett. **62**, 2179 (1993).
[22] I.H. Malitson, J. Opt. Soc. Am. **55**, 1205 (1965).